Defect Processes in Halogen Doped SnO₂

Petros-Panagis Filippatos [1,2], **Nikolaos Kelaidis** [2,3] (ID), **Maria Vasilopoulou** [1,*], **Dimitris Davazoglou** [1] **and Alexander Chroneos** [2,4] (ID)

1. Institute of Nanoscience and Nanotechnology (INN), National Center for Scientific Research Demokritos, 15341 Agia Paraskevi, GR-11635 Athens, Greece; filippap@uni.coventry.ac.uk (P.-P.F.); d.davazoglou@inn.demokritos.gr (D.D.)
2. Faculty of Engineering, Environment and Computing, Coventry University, Priory Street, Coventry CV1 5FB, UK; ad1978@coventry.ac.uk (N.K.); alexander.chroneos@imperial.ac.uk (A.C.)
3. Theoretical and Physical Chemistry Institute, National Hellenic Research Foundation, Vass. Constantinou 48, GR-11635 Athens, Greece
4. Department of Materials, Imperial College, London SW7 2AZ, UK
* Correspondence: m.vasilopoulou@inn.demokritos.gr

Abstract: In the present study, we performed density functional theory calculations (DFT) to investigate structural changes and their impact on the electronic properties in halogen (F, Cl, Br, and I) doped tin oxide (SnO₂). We performed calculations for atoms intercalated either at interstitial or substitutional positions and then calculated the electronic structure and the optical properties of the doped SnO₂. In all cases, a reduction in the bandgap value was evident, while gap states were also formed. Furthermore, when we insert these dopants in interstitial and substitutional positions, they all constitute a single acceptor and donor, respectively. This can also be seen in the density of states through the formation of gap states just above the valence band or below the conduction band, respectively. These gap states may contribute to significant changes in the optical and electronic properties of SnO₂, thus affecting the metal oxide's suitability for photovoltaics and photocatalytic devices. In particular, we found that iodine (I) doping of SnO₂ induces a high dielectric constant while also reducing the oxide's bandgap, making it more efficient for light-harvesting applications.

1. Introduction

SnO₂ is a wide bandgap, n-type semiconductor that adopts a tetragonal crystal structure [1–6]. Doping is also used to increase further its electrical conductivity as well as its transparency in the visible region [4–6]. SnO₂ is mainly used as an opacifier of glazes [1], polishing powder [2], protective polymer coating [3], as a functional material in the solar cell technology [4], transparent conducting oxide [5,6] and gas sensor [7]. Recently Zhao et al. [8] demonstrated that a NO gas sensor based on Sn₂O₃ has an improved selectivity to NO, NO₂, and CO gases [8]. Wang et al. [9] have shown that Sn₃O₄ in ultrathin SnO₂ nanosheets exhibits great performance for Li-ion storage for battery technology. Furthermore, there are many experiments that examine the effect of halogen doping in SnO₂ thin films with fluorine (F) being the most commonly used dopant because it significantly increases the conductivity and transparency of SnO₂, hence making it appropriate for use as the transparent electrode in several classes of optoelectronics [10–14]. These include the sol-gel preparation of F:SnO₂ nanostructures [11], studies on the structural characteristics, and the changes through the fluorine doping using X-ray diffraction (XRD) techniques [12] as well as deposition methods, such us spray pyrolysis [13] and chemical vapor deposition [14,15] for producing the F:SnO₂. Regarding the F doping mechanism, several studies on F-doped SnO₂ nanopowders using X-ray diffraction (XRD) analysis, transmission electron microscopy (TEM), X-ray photoelectron spectroscopy (XPS), and Fourier transformed

infrared spectroscopy (FTIR) [16] revealed that at low concentration, F atoms occupy oxygen vacancy sites as substitutional dopants, but for higher concentrations F atoms site in interstitial positions in the host lattice. Moreover, few reports have also demonstrated the effects of chlorine (Cl), bromine (Br), and I doping in SnO_2. Abass et al. [17–19], using several experiments with emphasis on optical and electrical properties, found pronounced improvements in these properties by halogen doping. Agashe et al. [20] also studied the electrical properties of sprayed deposited SnO_2 films and showed that when replacing F dopants with Br, conductivity was reduced.

Except for experimental studies, there are also many theoretical research efforts using DFT that examine the role of defects such as F, Sb, and Cl in substitutional positions in SnO_2 [21–27]. They revealed that such doping contributes to the formation of single donor states; however, the effect of interstitially doped SnO_2 has not been studied yet. Additionally, the influence of other halogen dopants (besides F, Cl) in SnO_2 and the corresponding changes in the oxide's band structure and optical properties have not been systematically investigated yet. In most previously published DFT studies, the bandgap is significantly underestimated within the range 1 eV–2 eV [27–29]. This is a common problem when DFT calculations on wide bandgap semiconductors are conducted [30,31]. As a result, a number of methods have been developed in order to calculate more accurately the bandgap of these materials, with the Hubbard + U correction method and the computationally demanding but more accurate hybrid pseudopotentials being the most commonly used. Many researchers have applied the Hubbard + U method for the d orbitals of Sn, but still, the band gap was substantially underestimated (2.5 eV). In the case of hybrid pseudopotentials, although the band gap reaches the correct experimental value of 3.7 eV [32], the computational cost is very high, and this is why the majority of these researchers use a small number of atoms in their unit cells [33].

In the present study, we investigate the halogen doping of the bulk SnO_2 using DFT in order to examine changes in the electronic structure as well as improvements in the photocatalytic properties of SnO_2. To achieve such an endeavor, we apply hybrid DFT calculations. With this method, the bandgap reaches the correct value of 3.35 eV and it is in good agreement with similar DFT works [34]. We examined all the possible defect sites for the halogen dopants and we also calculated the minimum energies for these dopants being at interstitial positions and the changes in the electrical properties. Using the total density of states (DOS) and the projected density of states (pDOS), we analyzed the minimum energy sites of the defects and their effect on the bandgap. Furthermore, we predicted the optical properties of all the doping cases and we compared our results with the available experimental data.

2. Methodology

For the DFT calculations, we used the Cambridge Serial Total Energy Package (CASTEP) [35,36]. DFT calculations were performed using the Local Density Approximation (LDA) exchange-correlation Functional [37] with ultrasoft pseudopotentials [38]. The cutoff energy that met the convergence criteria was chosen at 800 eV and also for the geometry optimization of a 48 atom supercell, a $2 \times 2 \times 3$ Monkhorst-Pack (MP) k-points set [39] was selected with the Broyden-Fletcher-Goldfard-Shanno (BFGS) method. As it was previously described, to consider the effects of the localized electrons, we used the hybrid functional PBE0 [39], which overcomes the LDA band gap error. Lastly, the DOS calculations were performed using a $3 \times 3 \times 3$ k points mesh and the pDOS were performed using a k point mesh of $7 \times 7 \times 7$. The convergence criteria for our analyses were chosen as 0.05 eV/Å for the Max force tolerance, 0.001 Å for the Max displacement tolerance, 0.1 GPa for the Max stress tolerance, and 2.0×10^{-5} eV/atom for the SCF tolerance.

3. Results

3.1. Structural Properties

SnO_2 has a rutile structure and it belongs to the space group of $P4_2/mmm$ (space group no 136) of the tetragonal system. The calculated lattice parameters of the unit cell are a = b = 4.717 Å and c = 3.189 Å ($\alpha = \beta = \gamma = 90°$), in good agreement with the experimental results (a = 4.737 Å and c = 3.186 Å) [40]. In Figure 1a–h, the geometry of doped SnO_2 structures is presented for the examined dopants (F, Cl, Br, and I) in substitutional and interstitial positions, where in each case the local distortion of the lattice is shown. The respective lattice parameters are presented in Table 1. An increase of cell dimensions due to the halogen incorporation in the SnO_2 lattice is observed, as the substitution of oxygen with a larger atom (all halogens have a larger atomic radius than oxygen) will distort the lattice, increasing total volume, more so in the case of interstitial doping. It is interesting to note that in the case of iodine at an interstitial position, I_i, the cell increases in volume as both a and b increase, but the c parameter decreases. The anisotropic changes in the lattice parameters upon the introduction of the I atom is due to the reduction in the c-direction of the Sn-Ii bond length (3.31 Å) as compared to the Sn-I bond before our optimization (3.40 Å).
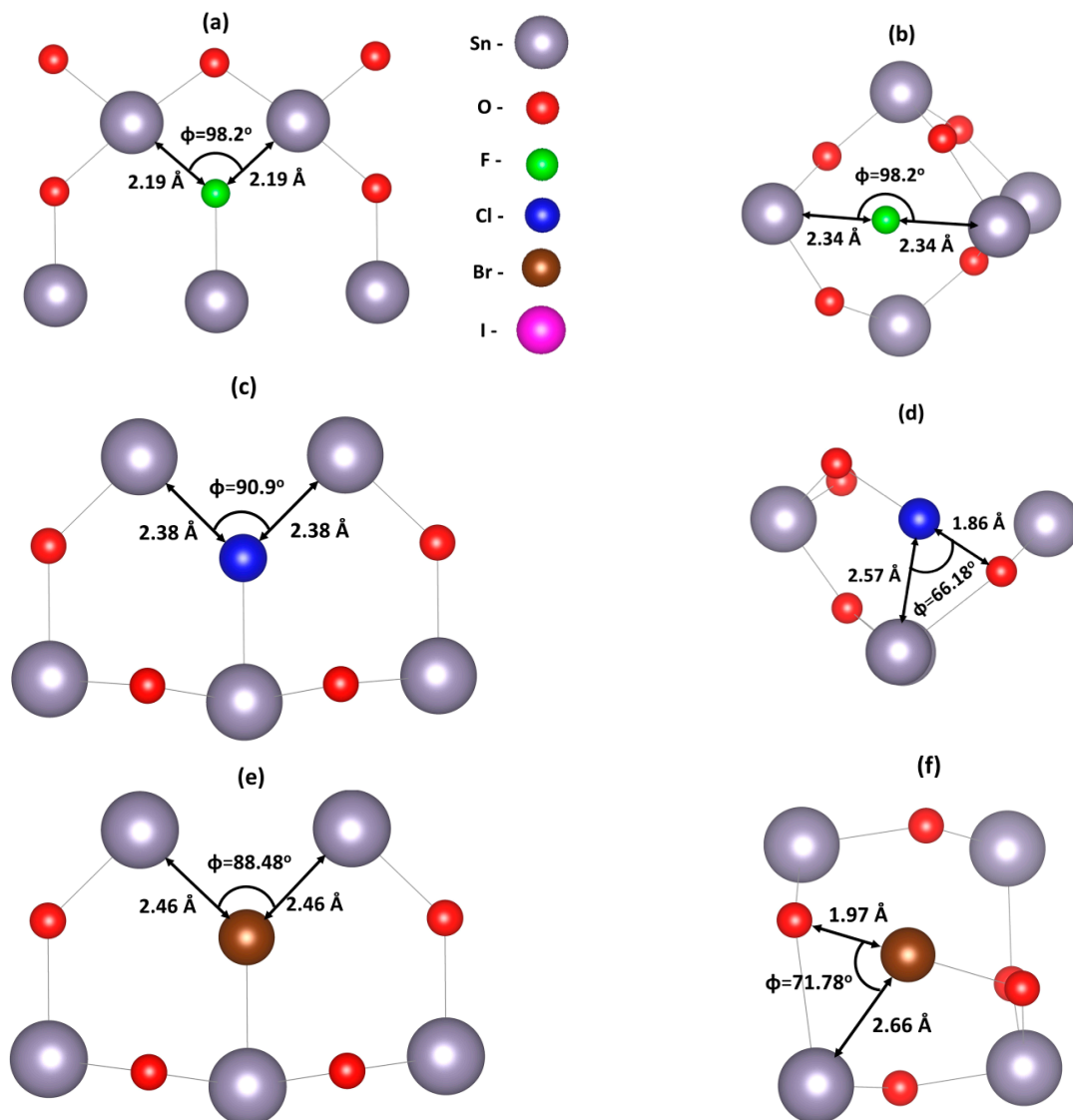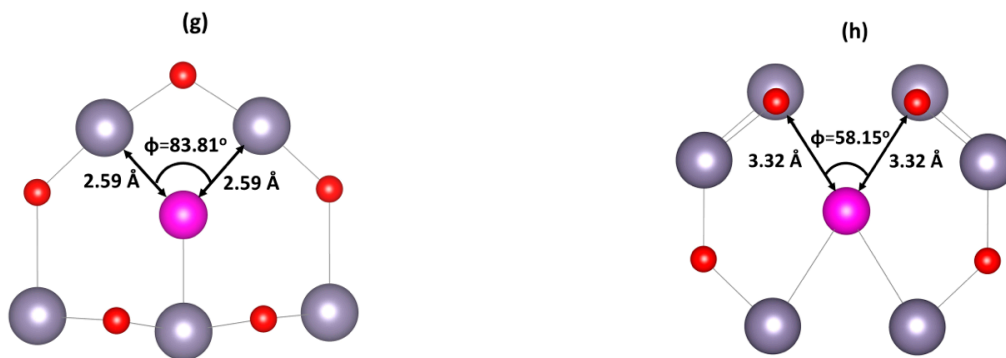

Figure 1. *Cont.*

Figure 1. (**a**) F_o: SnO_2, (**b**) F_i: SnO_2, (**c**) Cl_o: SnO_2, (**d**) Cl_i: SnO_2, (**e**) Br_o: SnO_2, (**f**) Br_i: SnO_2, (**g**) I_o: SnO_2, (**h**) I_i: SnO_2.

Table 1. The computed lattice parameters and cell volumes for every doping case.

	a (Å)	b (Å)	c (Å)	Vol (Å^3)
SnO_2	4.717	4.717	3.189	70.956
F_i: SnO_2	4.739	4.715	3.195	71.390
Fo: SnO_2	4.735	4.735	3.205	71.857
Cl_i: SnO_2	4.789	4.790	3.201	73.429
$Cl_o SnO_2$	4.778	4.778	3.213	73.350
Br_i: SnO_2	4.795	4.845	3.194	74.202
Br_o: SnO_2	4.795	4.795	3.218	73.988
I_i: SnO_2	5.055	4.830	3.165	77.276
I_o: SnO_2	4.840	4.840	3.215	75.313

3.2. Electrical Properties

We examine the effect of halogen doping on the electronic properties and band gap of SnO_2 by calculating the Density of States (DOS) of perfect and doped SnO_2.

The bandgap of the undoped SnO_2 is calculated using the PBE0 functional, at 3.35 eV (Figure 2a) close (but still underestimated) to the experimental value of 3.7 eV [32], in agreement with other theoretical studies [41–43]. As it is observed from Figure 2b, the F interstitial in SnO_2 gives rise to energy states inside the band gap, near the band edges with a small reduction of 0.2 eV of the bandgap width, calculated at 3.12 eV (Figure 2b). When F is situated in an O-substitutional position, the bandgap is notably reduced to 2.90 eV without the presence of gap states (Figure 2c).
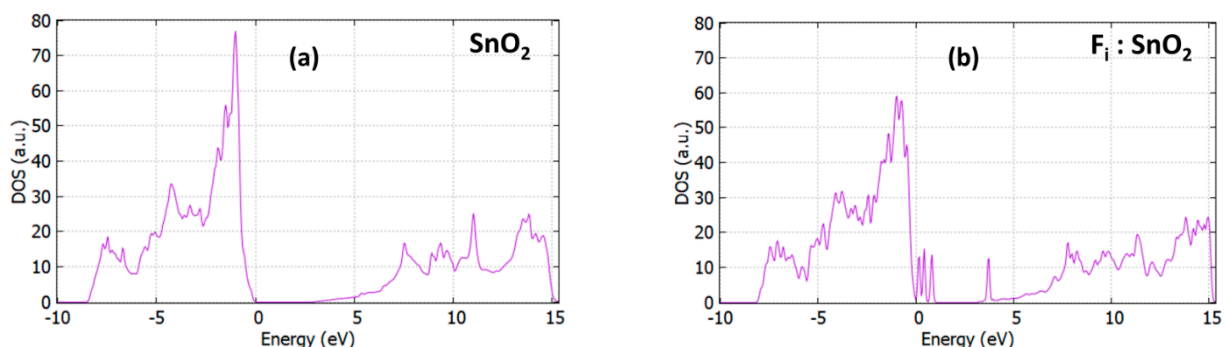

Figure 2. *Cont.*
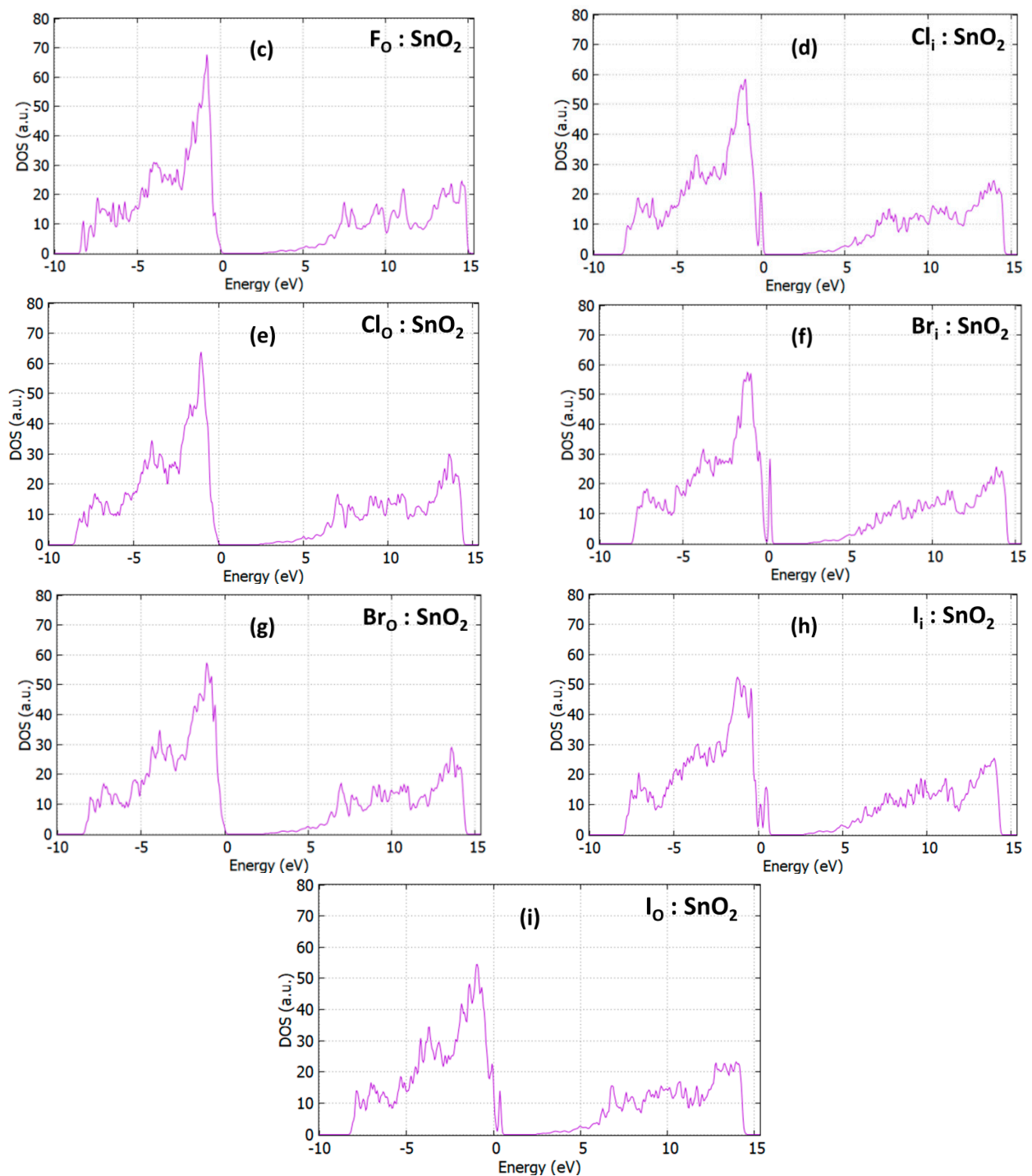
Figure 2. The Density of States (DOS) of the (**a**) undoped SnO_2, (**b**) F_i doped SnO_2, (**c**) Fo doped SnO_2, (**d**) Cl_i doped SnO_2, (**e**) Clo doped SnO_2, (**f**) Br_i doped SnO_2, (**g**) Br_O doped SnO_2, (**h**) I_i doped SnO_2, and (**i**) I_O doped SnO_2.

Regarding the Cl doping, in the case of interstitial doping, Cl_i: SnO_2, the bandgap is further reduced to 2.85 eV with gap states present near the valence band. When Cl is at an O-substitutional position, Cl_o, a more significant bandgap reduction occurs, to 2.70 eV (Figure 2d,e). In a previous DFT research on F and Cl doped TiO_2 [44], we also observed a significant bandgap reduction when a Cl atom was inserted in an interstitial position.

Regarding the effect of a Br interstitial intercalation (Figure 2f), the calculated bandgap is reduced to 2.90 eV with gap states near the valence band edge (minimum) are created. In comparison, in the case of substitutional Br_o, the bandgap reaches a value of 2.71 eV

(Figure 2g). It is evident that regarding the electronic structure, Br doping has the same effect as Cl doping in terms of bandgap reduction.

Lastly, I interstitial and substitutional doping is examined. We calculated that the bandgap is reduced to a value of 2.62 eV for the interstitial and 2.61 eV for the substitutional case, respectively, while states near the valence band are again presented. In this case, the substitutional doping has a smaller bandgap value than the interstitial case. This can be attributed to the states that are created to the valence band edge, which is due to the hybridization of the 2p orbitals of the nearest oxygen atom with the iodine 5p orbitals. As iodine is larger than the other halogens, even in the substitutional position, its orbitals are mixing with the nearest oxygen atom, giving rise to the states near the valence band. These results indicate that halogen interstitial dopants serve as single acceptors when they are intercalated within the SnO_2 host lattice. Such gap states near the oxide's valence band maximum and those near the conduction band position may act as shallow and deep acceptors, respectively, hence contributing to performance enhancements of devices based on doped SnO_2. However, the gap states may also act as traps for the photogenerated carriers in specific photovoltaic devices such as organic and halide perovskite photovoltaics, thus decreasing the device photocurrent and overall performance.

However, the incorporation of substitutional halogen atoms in oxygen position does not introduce any gap states. This is in stark contrast with the intercalation of interstitial halogens that create some localized perturbations upon the upper valence band and the conduction band of the material. That implies free electrons' presence contributing to the n-type conductivity, in accordance with experimental observations [45–48]. The halogen substitutional doping is seen to induce states inside or near the valence band. We believe that this can be explained because in the substitutional doping, the halogen orbitals are not mixing with the nearest Sn-5p or O-2p orbitals. As a result, no hybridized mid-gap states arise.

In Table 2 we have summarized our results. According to these calculations, the minimum value of the calculated bandgap is 2.61 eV for the case of I_o doping. It is therefore suggested as the most effective of the halogen SnO_2 dopants for photocatalytic applications.

Table 2. Band gap values for every halogen doping case.

Halogen Dopants	Band Gap	
	Interstitial Doping	Substitutional Doping
F	3.12	2.90
Cl	2.85	2.70
Br	2.90	2.71
I	2.62	2.61

Therefore, it is suggested that this type of doping can be used to develop better photocatalysts.

In Figures 3 and 4, the pDOS for the doped SnO_2 are shown. From the pDOS, we can gain important information about the gap states and the contribution of each element's orbitals to the valence and conduction band. As seen in Figure 3a, which shows the pDOS of the plain SnO_2, the valence band is mainly consisting of O-2p and Sn-5p orbitals, whereas the conduction band is created from the Sn-5s, Sn-5p, O-2s, and O-2p. This is in good agreement with previous theoretical studies [41,42]. Referring to Figure 3b, we see that F doped SnO_2 has a similar valence and conduction band structure with the undoped SnO_2 with a small deviation coming from the contribution of fluorine in the doped oxide. Focusing on the gap states formed near the valence band in the F-doped material, calculations show that it is created due to the hybridization of O-2p with F-2p orbitals (refer to Figure 4a). This is the same phenomenon that we predicted to occur in the case of TiO_2 [43] upon doping with interstitial F atoms.
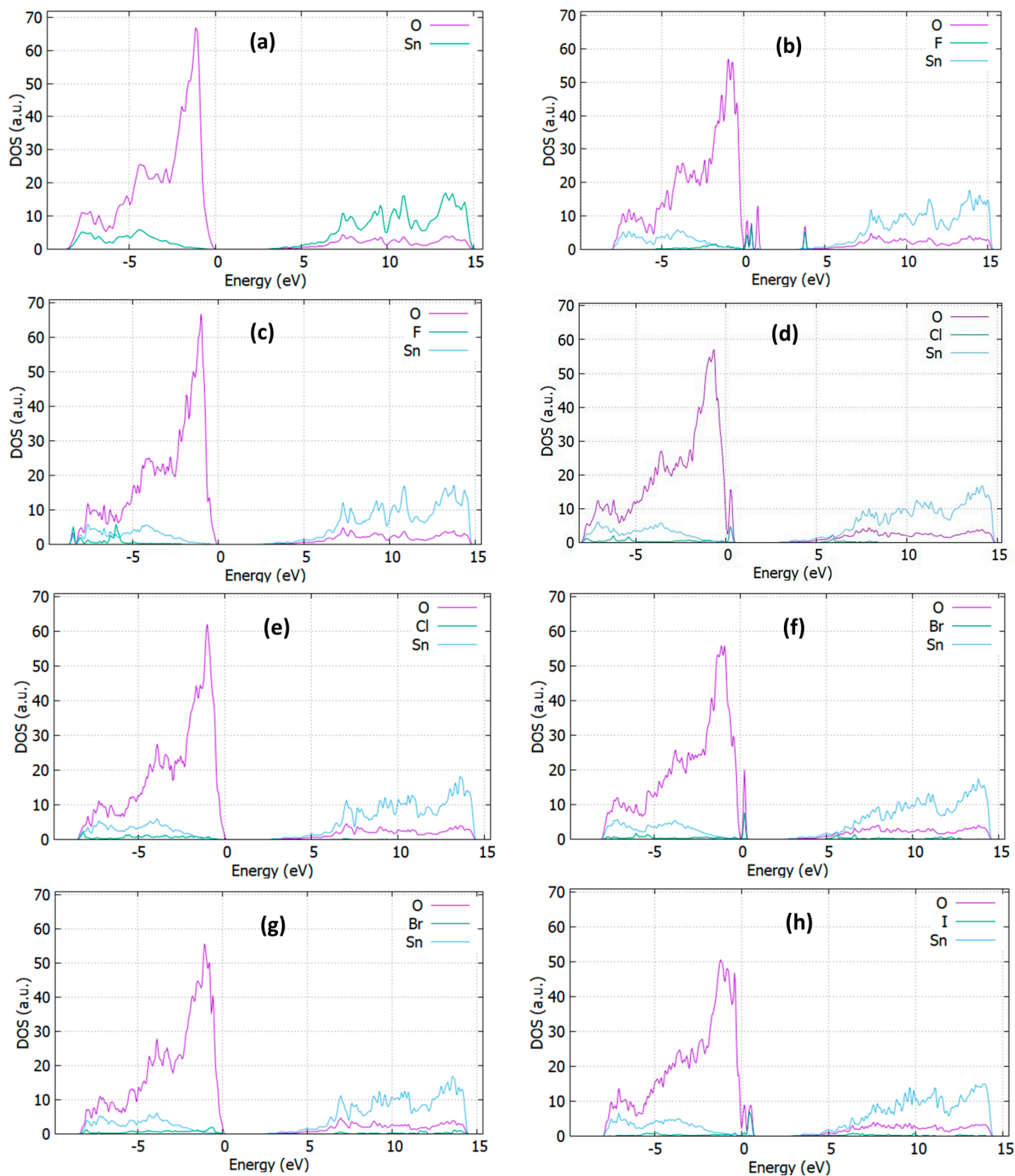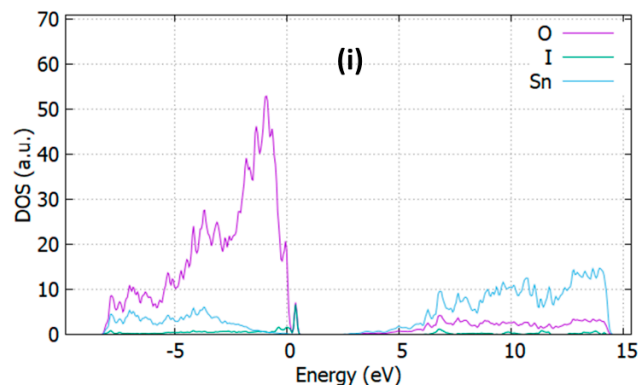
Figure 3. *Cont.*

Figure 3. pDOS graphs of (**a**) undoped SnO_2, (**b**) F_i doped SnO_2, (**c**) Fo doped SnO_2, (**d**) Cl_i doped SnO_2, (**e**) Clo doped SnO_2, (**f**) Br_i doped SnO_2, (**g**) Br_O doped SnO_2, (**h**) I_i doped SnO_2, and (**i**) I_O doped SnO_2.
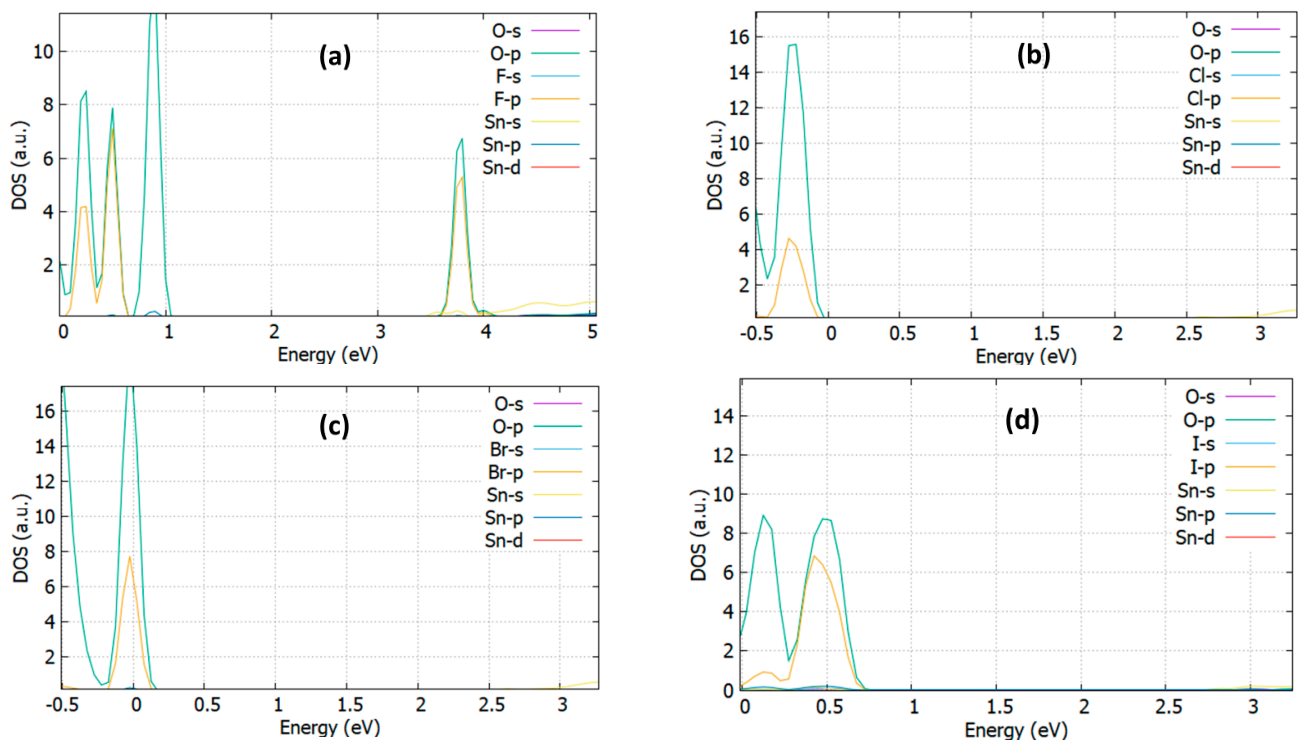
Figure 4. (**a**) The gap states of the F_i doped SnO_2; (**b**) The gap states of the Cl_i doped SnO_2; (**c**) The gap states of Br_i doped SnO_2; (**d**) The gap states of I_i doped SnO_2.

Similarly, in Figure 4b–d the rise of gap states is mainly created by the O-2p and Cl-2p and O-2p and Br-4p and I-5p. This probably indicates that the formation of mid-gap states in halogen doped n-type metal oxides such as SnO_2 and TiO_2 may have a universal origin. In any case, further investigation is needed, which is beyond the scope of the present manuscript.

3.3. Optical Properties

The complex dielectric function can provide important information concerning the polarization mechanisms of the solid. The dominant dispersion/absorption mechanisms in the visible and ultraviolet range are caused by electronic excitations, i.e., transitions from occupied to empty electron levels. The dielectric function can describe these transitions.

In Figure 5a, the complex dielectric function of undoped SnO_2 is presented. The real part of the dielectric function of the undoped SnO_2 is descended as we increase the energy, reaching a maximum at 8.5 eV. The negative value in the energy range from 16–17 eV

indicates that SnO_2 has metallic properties [49,50]. The probability of photon absorption is calculated through the imaginary part of the dielectric function. Specifically, we observe two major peaks at 10 eV and at 12.5 eV, which are assigned to the electronic interband transition from O-2p to Sn 5p. The dielectric constant for the undoped case is calculated to 2, which agrees well with the experimental value of 1.6 [49] and similar DFT works predict a value of 2 [50]. In Figure 5b–i, all the dielectric functions for the doped cases are shown. It is evident that in the case of the interstitial doping with F, there is a notable improvement to the dielectric constant as it reaches the value of 3.2 from the real part of the dielectric function. The existence of a major peak at 1 eV can be attributed to the electronic transition of F-2p and the Sn-5p in the conduction band. As regards the other interstitial cases, it is predicted that the dielectric constant is almost unchanged except the I_i: SnO_2, which shows an improvement, and it reaches a value of 2.7. For the substitutional doping cases, in the case of I_o: SnO_2, we calculate that the maximum value of the dielectric constant is achieved, which is 2.4.
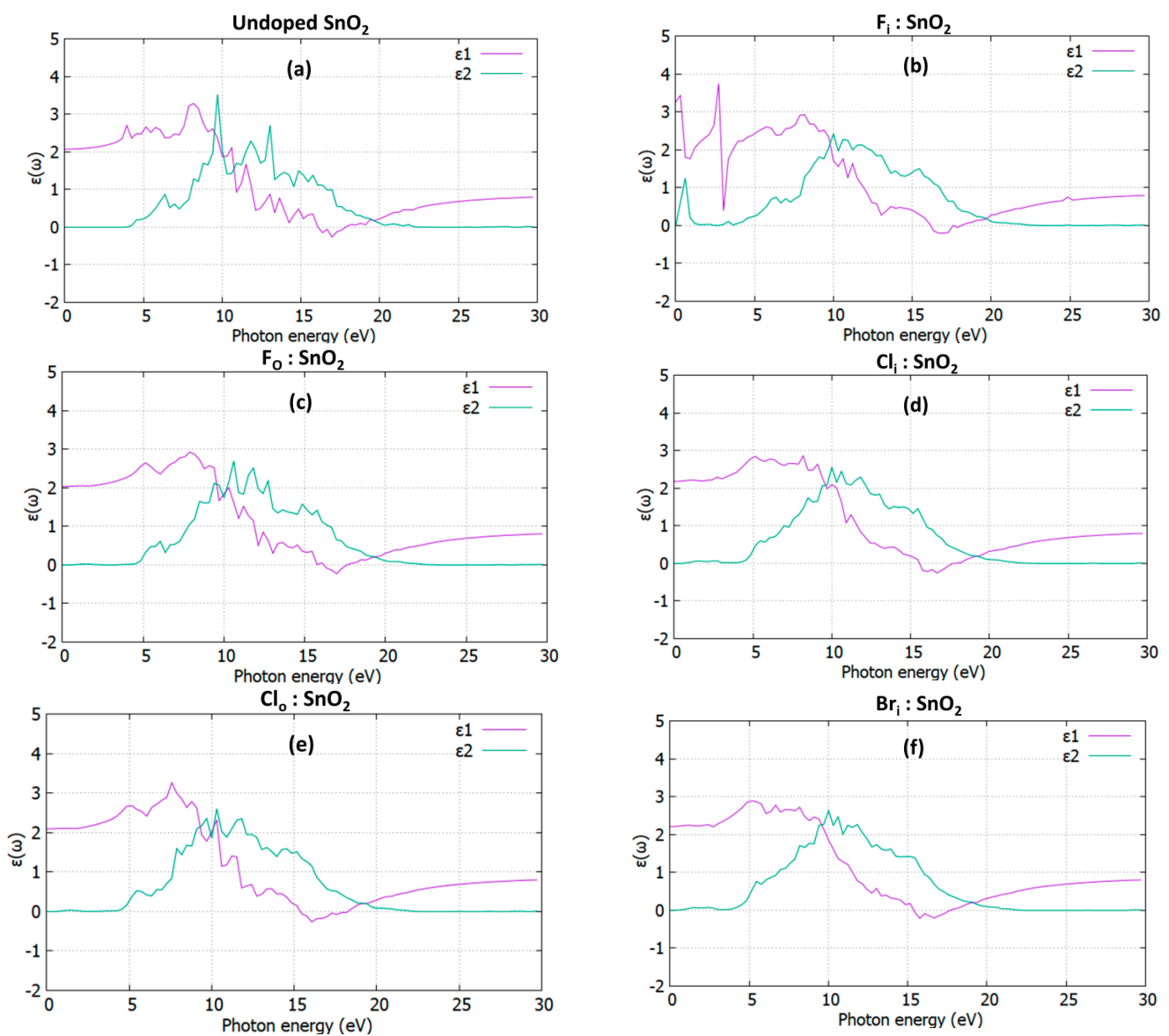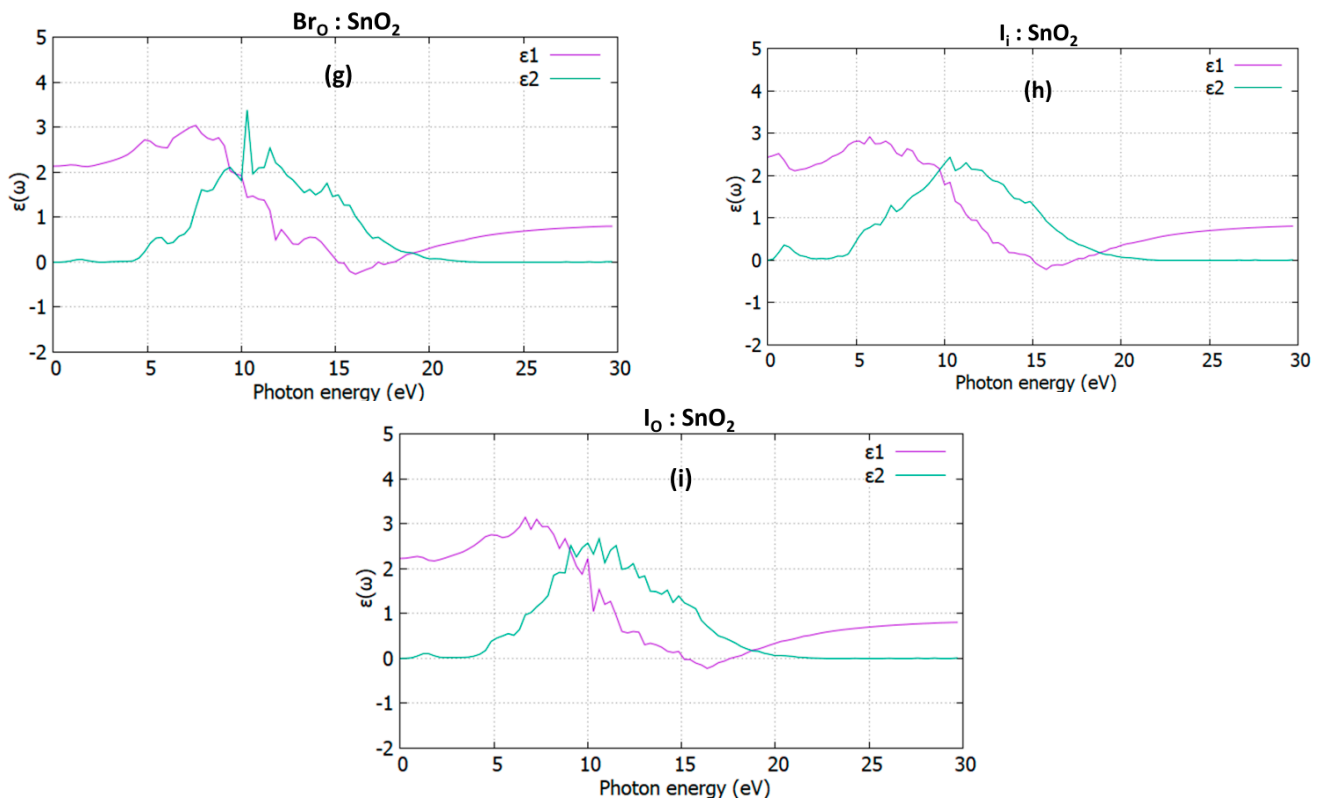

Figure 5. *Cont.*

Figure 5. The dielectric function of the (**a**) undoped SnO$_2$, (**b**) Fi doped SnO$_2$, (**c**) Fo doped SnO$_2$, (**d**) Cli doped SnO$_2$, (**e**) Clo doped SnO$_2$, (**f**) Br$_i$ doped SnO$_2$, (**g**) Br$_O$ doped SnO$_2$, (**h**) I$_i$ doped SnO$_2$, and (**i**) I$_O$ doped SnO$_2$.

The calculated refractive index (refer to Figure 6) for the undoped SnO$_2$ is 1.40. This result is more underestimated than the experimental value of 1.70 [51], but agrees well with the value of other DFT studies [50]. The extinction coefficient can be described through the imaginary part of the refractive index, k. The major peak at the imaginary part of the undoped case is located at 12.5 eV. For the interstitial cases, we calculated that F$_i$ shows an increase at the refractive index and reaches a value of 1.8. Afify et al. [52] experimentally predicted that the refractive index of F: SnO$_2$ was between 1.85–2.2, which agrees well with the present study. For the substitutional cases, the refractive index has its maximum value of 1.51 in the case of Io: SnO$_2$. The increase of the refractive index for Fi and Io boosts the antireflectivity (AR) of SnO$_2$ and might be beneficial for application in energy harvesting devices.
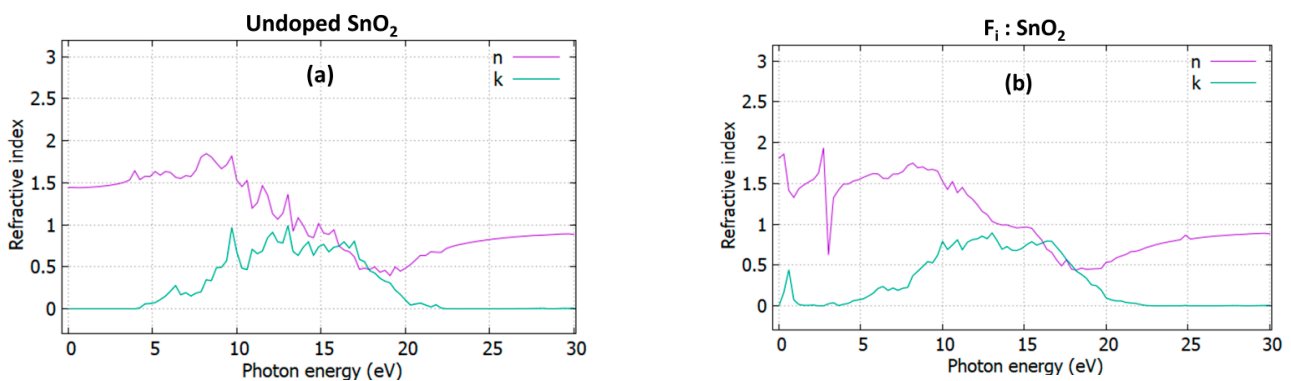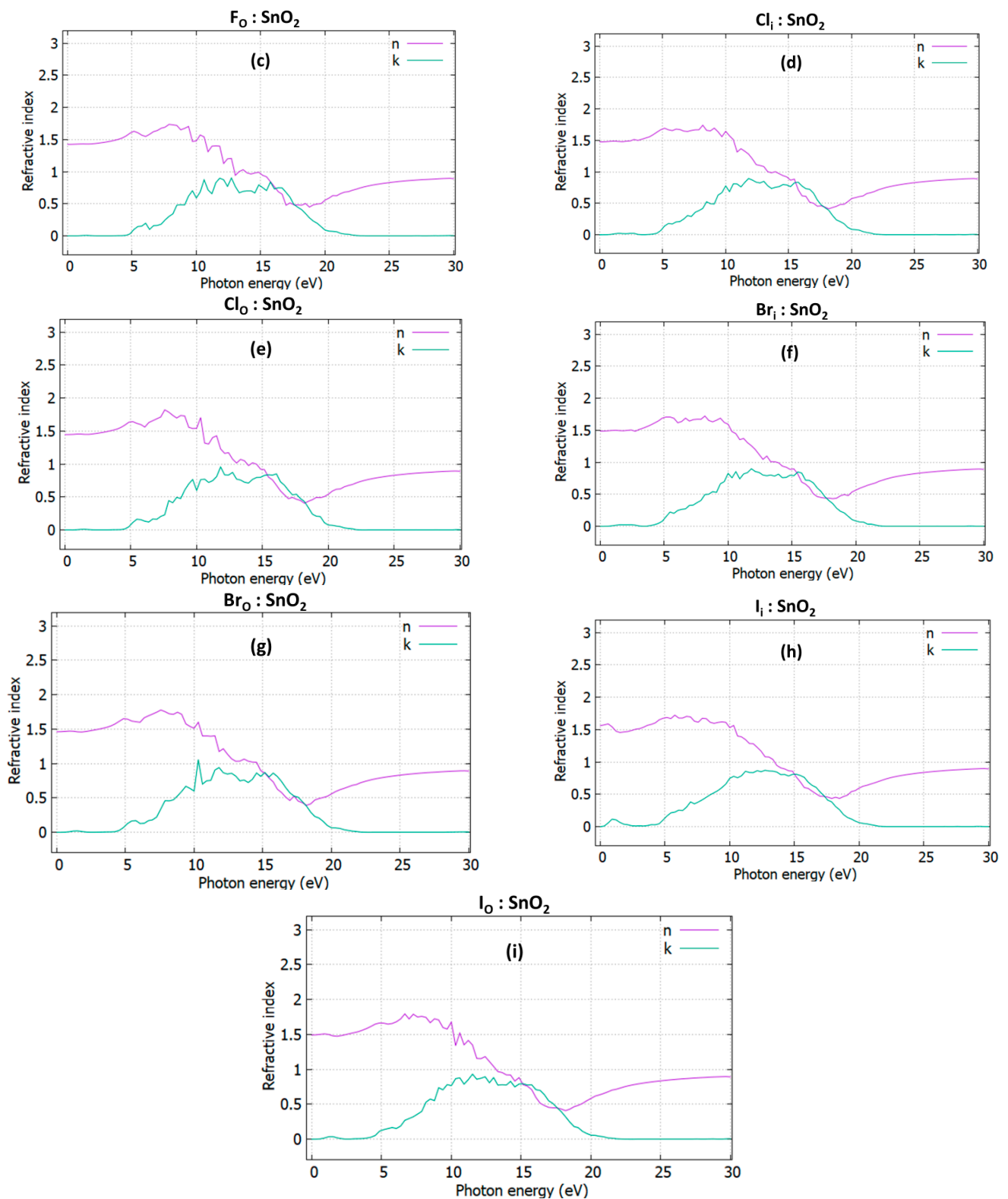

Figure 6. *Cont.*

Figure 6. The refractive index of the (**a**) plain SnO_2, (**b**) F_i doped SnO_2, (**c**) F_o doped SnO_2, (**d**) Cl_i doped SnO_2, (**e**) Clo doped SnO_2, (**f**) Bri doped SnO_2, (**g**) Br_O doped SnO_2, (**h**) I_i doped SnO_2, and (**i**) I_O doped SnO_2.

Lastly, the absorption co-efficiency is presented in Figure 7. The major peaks range from 5 eV to 22 eV, and it is in good agreement with previous DFT studies [50]. The absorption of pure SnO_2 starts at 380 nm, which is somewhat underestimated than the experimental value, which is around 400 nm [52]. It is seen that in the visible region

(1.78–3.12 eV), I doped SnO$_2$ has the highest absorption both for the interstitial and the substitutional positions.
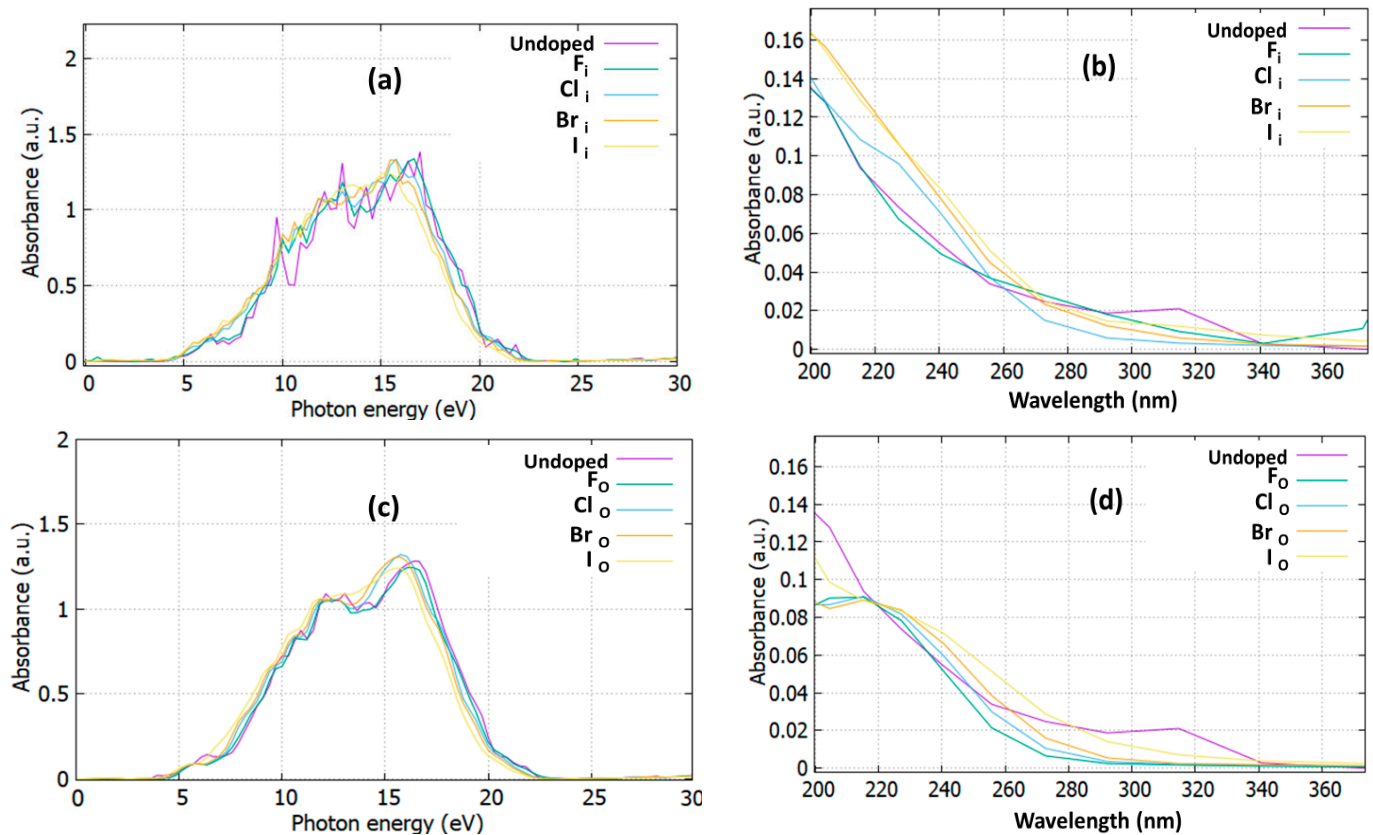

Figure 7. The absorption for (**a**) interstitially doped SnO$_2$ for all the energy spectrum, (**b**) interstitially doped SnO$_2$ as a function of the wavelength, (**c**) substitutionally doped SnO$_2$ for all the energy spectrum, (**d**) substitutionally doped SnO$_2$ as a function of the wavelength.

4. Conclusions

DFT calculations were performed for halogen doped SnO$_2$ and the effects of the exact kind of doping on the bandgap value and electronic properties were discussed. In this research, interstitial and substitutional halogen defects were examined. In all cases, it was observed that gap states were created from hybridization of O-2p with halogen 1s orbitals. Such energy states are beneficial for the oxide's photocatalytic activity as they significantly reduce the optical band gap concerning that of undoped SnO$_2$. They can also serve as charge transport paths in a certain type of optoelectronic device, whereas this might be detrimental for the application of halogen-doped oxide as electron transport material in other classes of photovoltaic devices. Iodine doped SnO$_2$ has the lowest bandgap value of 2.60 eV and it is one of the lowest values reported for SnO$_2$. Interestingly, when iodine resides in an oxygen site, it has a better refractive index and absorbance than the other halogen dopants. This makes it a suitable dopant candidate for SnO$_2$-based energy harvesting devices.

Author Contributions: P.-P.F. and N.K. performed the DFT calculations, P.-P.F., N.K., M.V., A.C., wrote the paper, M.V., A.C. and D.D. contributed in the analysis and discussion of the results. All authors have read and agreed to the published version of the manuscript.

Institutional Review Board Statement: Not applicable.

Informed Consent Statement: Not applicable.

Data Availability Statement: Not applicable.

Conflicts of Interest: The authors declare no conflict of interest.

References

1. Searle, A.B. *The Glazer's Book*; The Technical Press: London, UK, 1935.
2. Holleman, A.F.; Wiberg, E. *Inorganic Chemistry*; Academic Press: Cambridge, MA, USA, 2001.
3. Greenwood, N.N.; Earnshaw, A. *Chemistry of the Elements*; Elsevier: Amsterdam, The Netherlands, 2012.
4. Tountas, M.; Topal, Y.; Kus, M.; Ersöz, M.; Fakis, M.; Argitis, P.; Vasilopoulou, M. Water-Soluble Lacunary Polyoxometalates with Excellent Electron Mobilities and Hole Blocking Capabilities for High Efficiency Fluorescent and Phosphorescent Organic Light Emitting Diodes. *Adv. Funct. Mater.* **2016**, *26*, 2655–2665. [CrossRef]
5. Batzill, M.; Diebold, U. The Surface and Materials Science of Tin Oxide. *Prog. Surf. Sci.* **2005**, *79*, 47–154. [CrossRef]
6. Fortunato, E.; Ginley, D.; Hosono, H.; Paine, D.C. Transparent conducting oxides for photovoltaics. *MRS Bull.* **2007**, *32*, 242–247. [CrossRef]
7. Göpel, W.; Schierbaum, K.D. SnO_2 sensors: Current status and future prospects. *Sens. Actuators B Chem.* **1995**, *26*, 1–12. [CrossRef]
8. Zhao, J.; Tan, R.; Shen, W.; Yang, Y.; Guo, Y.; Li, J.; Zhou, Z.; Jian, J.; Song, W. Highly selective Sn_2O_3-based sensors for NO detection. *Mater. Lett.* **2012**, *84*, 94–96. [CrossRef]
9. Wang, C.; Du, G.; Ståhl, K.; Huang, H.; Zhong, Y.; Jiang, J.Z. Ultrathin SnO_2 nanosheets: Oriented attachment mechanism, nonstoichiometric defects, and enhanced lithium-ion battery performances. *J. Phys. Chem. C* **2012**, *116*, 4000–4011. [CrossRef]
10. Rakhshani, A.E.; Makdisi, Y.; Ramazaniyan, H.A. Electronic and optical properties of fluorine-doped tin oxide films. *J. Appl. Phys.* **1998**, *83*, 1049–1057. [CrossRef]
11. Wu, S.; Yuan, S.; Shi, L.; Zhao, Y.; Fang, J. Preparation, characterization and electrical properties of fluorine-doped tin dioxide nanocrystals. *J. Coll. Interface Sci.* **2010**, *346*, 12–16. [CrossRef]
12. Garces, F.A.; Budini, N.; Koropecki, R.R.; Arce, R.D. Structural mosaicity and electrical properties of pyrolytic SnO_2:F thin films. *Thin Solid Films* **2013**, *531*, 172–178. [CrossRef]
13. Elangovan, E.; Ramamurthi, K. A study on low cost-high conducting fluorine and antimony-doped tin oxide thin films. *Appl. Surf. Sci.* **2005**, *249*, 183–196. [CrossRef]
14. Yang, J.; Liu, W.; Dong, L.; Li, Y.; Li, C.; Zhao, H. Studies on the structural and electrical properties of F-doped SnO_2 film prepared by APCVD. *Appl. Surf. Sci.* **2011**, *257*, 10499–10502. [CrossRef]
15. Moholkar, A.V.; Pawar, S.M.; Rajpure, K.Y.; Bhosale, C.H.; Kim, J.H. Effect of fluorine doping onhighly transparent conductive spray deposited nanocrystalline tin oxide thin flms. *Appl. Surf. Sci.* **2009**, *255*, 9358–9364. [CrossRef]
16. Suffner, J.; Ágoston, P.; Kling, J.; Hahn, H. Chemical vapor synthesis of fluorine-doped SnO_2 (FTO) nanoparticles. *J. Nanopart. Res.* **2010**, *12*, 2579–2588. [CrossRef]
17. Abass, A.K. Electrical and optical properties of chlorine doped SnO_2 coatings. *Solid State Commun.* **1987**, *61*, 507–510. [CrossRef]
18. Abass, A.K.; Bakr, H.; Jassim, S.A.; Fahad, T.A. Electrical and optical properties of chemically deposited SnO_2: I coatings. *Sol. Energy Mater.* **1988**, *17*, 425–431. [CrossRef]
19. Abass, A.K.; Al-Liabi, N.A.; Taha, W.A. Optical properties of bromine-doped SnO_2 coatings for solar applications. *Phys. Status Solidi (a)* **1988**, *106*, 613–618. [CrossRef]
20. Agashe, C.; Major, S.S. Effect of F, Cl and Br doping on electrical properties of sprayed SnO_2 films. *J. Mater. Sci. Lett.* **1996**, *15*, 497–499. [CrossRef]
21. Peng-Fei, L.; Yue, S.; Zhong-Yuan, Y.; Long, Z.; Qiong-Yao, L.; Shi-Jia, L.M.; Li-Hong, H.; Yu-Min, L. Electronic structure and optical properties of antimony-doped SnO_2 from first-principle study. *Commun. Theor. Phys.* **2012**, *57*, 145.
22. Canestraro, C.D.; Roman, L.S.; Persson, C. Polarization dependence of the optical response in SnO_2 and the effects from heavily F doping. *Thin Solid Films* **2009**, *517*, 6301–6304. [CrossRef]
23. Rivera, R.; Marcillo, F.; Chamba, W.; Puchaicela, P.; Stashans, A. SnO_2 physical and chemical properties due to the impurity doping. *Lect. Notes Eng. Comp.* **2013**, *2*, 814–818.
24. Velikokhatnyi, O.I.; Kumta, P.N. Ab-initio study of fluorine-doped tin dioxide: A prospective catalyst support for water electrolysis. *Physica B* **2011**, *406*, 471–477. [CrossRef]
25. Golovanov, V.; Golovanova, V.; Kuisma, M.; Rantala, T.T. Electron spin resonance parameters of cation vacancies in tin dioxide doped with fluorine and hydrogen. *J. Appl. Phys.* **2013**, *114*, 143907. [CrossRef]
26. Oshima, M.; Yoshino, K. Structural and Electronic Structure of SnO_2 by the First-Principle Study. *Mater. Sci. Forum* **2012**, *725*, 265–268. [CrossRef]
27. Govaerts, K.; Partoens, B.; Lamoen, D. Extended homologous series of Sn–O layered systems: A first-principles study. *Solid State Comm.* **2016**, *243*, 36–43. [CrossRef]
28. Marcillo, F.; Stashans, A. DFT calculations of tin dioxide crystals containing heavily-doped fluorine. *J. Theor. Comput. Chem.* **2014**, *13*, 1450069. [CrossRef]

29. Perdew, J.P.; Levy, M. Physical content of the exact Kohn-Sham orbital energies: Band gaps and derivative discontinuities. *Phys. Rev. Lett.* **1983**, *51*, 1884. [CrossRef]
30. Sham, L.J.; Schlüter, M. Density-functional theory of the energy gap. *Phys. Rev. Lett.* **1983**, *51*, 1888. [CrossRef]
31. Thangaraju, B. Structural and electrical studies on highly conducting spray deposited fluorine and antimony doped SnO_2 thin films from $SnCl_2$ precursor. *Thin Solid Films* **2002**, *402*, 71–78. [CrossRef]
32. Zervos, M.; Lathiotakis, N.; Kelaidis, N.; Othonos, A.; Tanasa, E.; Vasile, E. Epitaxial Highly Ordered Sb:SnO_2 Nanowires Grown by the Vapor Liquid Solid Mechanism on m-, r- and a-Al_2O_3. *Nanoscale Adv.* **2019**, *1*, 1980–1990. [CrossRef]
33. Deng, H.X.; Li, S.S.; Li, J. Quantum confinement effects and electronic properties of SnO_2 quantum wires and dots. *J. Phys. Chem. C* **2010**, *114*, 4841–4845. [CrossRef]
34. Payne, M.C.; Teter, M.P.; Allan, D.C.; Arias, T.A.; Joannopoulos, J.D. CASTEP 4.2 Academic version, licensed under the UKCP-MSI Agreement. *Rev. Mod. Phys.* **1992**, *64*, 1045–1097. [CrossRef]
35. Segall, M.D.; Lindan, P.J.; Probert, M.A.; Pickard, C.J.; Hasnip, P.J.; Clark, S.J.; Payne, M.C. First-principles simulation: Ideas, illustrations and the CASTEP code. *J. Phys. Cond. Matter* **2002**, *14*, 2717–2744. [CrossRef]
36. Ceperley, D.M.; Alder, B.J. Exchange-correlation potential and energy for density-functional calculation. *Phys. Rev. Lett.* **1980**, *45*, 567–581.
37. Vanderbilt, D. Soft self-consistent pseudopotentials in a generalized eigenvalue formalism. *Phys. Rev. B* **1990**, *41*, 7892–7895. [CrossRef]
38. Monkhorst, H.J.; Pack, J.D. Special points for Brillouin-zone integrations. *Phys. Rev. B* **1976**, *13*, 5188–5192. [CrossRef]
39. Paier, J.; Marsman, M.; Hummer, K.; Kresse, G.; Gerber, I.C.; Angyan, J.G. Screened hybrid density functionals applied to solids. *J. Chem. Phys.* **2006**, *124*, 154709. [CrossRef] [PubMed]
40. Xu, J.; Huang, S.; Wang, Z. First principle study on the electronic structure of fluorine-doped SnO_2. *Solid State Commun.* **2009**, *149*, 527–531. [CrossRef]
41. Yahla, H.; Boukra, A.; Belhakem, M.; Lippens, P.E. First-principles calculations of the electronic structure and Mössbauer parameters of Sb-doped SnO_2. *Solid State Commun.* **2009**, *149*, 2202–2206. [CrossRef]
42. Borges, P.D.; Scolfaro, L.M.; Alves, H.W.L.; da Silva, E.F. DFT study of the electronic, vibrational, and optical properties of SnO_2. *Theor. Chem. Acc.* **2009**, *126*, 39–44. [CrossRef]
43. Filippatos, P.P.; Kelaidis, N.; Vasilopoulou, M.; Davazoglou, D.; Lathiotakis, N.N.; Chroneos, A. Defect processes in F and Cl doped anatase TiO_2. *Sci. Rep.* **2019**, *9*, 19970. [CrossRef] [PubMed]
44. Ramaiah, K.S.; Raja, V.S. Structural and electrical properties of fluorine doped tin oxide films prepared by spray-pyrolysis technique. *Appl. Surf. Sci.* **2006**, *253*, 1451–1458. [CrossRef]
45. Yadav, A.A.; Masumdar, E.U.; Moholkar, A.V.; Neumann-Spallart, M.; Rajpure, K.Y.; Bhosale, C.H. Electrical, structural and optical properties of SnO_2:F thin films: Effect of the substrate temperature. *J. Alloys Compd.* **2009**, *488*, 350–355. [CrossRef]
46. Elangovan, E.; Ramamurthi, K. Studies on micro-structural and electrical properties of spray-deposited fluorine-doped tin oxide thin films from low-cost precursor. *Thin Solid Films* **2005**, *476*, 231–236. [CrossRef]
47. Chinnappa, L.; Ravichandran, K.; Saravanakumar, K.; Muruganantham, G.; Sakthivel, B. The combined effects of molar concentration of the precursor solution and fluorine doping on the structural and electrical properties of tin oxide films. *J. Mater. Sci. Mater. Electron.* **2001**, *22*, 1827–1834. [CrossRef]
48. Bakr, N.A.; Salman, S.A.; Ali, M.N. Effect of Fluorine Doping on Structural and Optical Properties of SnO_2 Thin Films Prepared by Chemical Spray Pyrolysis Method. *Adv. Mater.* **2006**, *5*, 23. [CrossRef]
49. Tingting, S.; Fuchun, Z.; Weihu, Z. Density functional theory study on the electronic structure and optical properties of SnO_2. *Rare Met. Mat. Eng.* **2015**, *44*, 2409–2414. [CrossRef]
50. Khan, A.F.; Mehmood, M.; Aslam, M.; Ashraf, M. Characteristics of electron beam evaporated nanocrystalline SnO_2 thin films annealed in air. *Appl. Surf. Sci.* **2010**, *256*, 2252–2258. [CrossRef]
51. Afify, H.H.; Momtaz, R.S.; Badawy, W.A.; Nasser, S.A. Some physical properties of fluorine-doped SnO_2 films prepared by spray pyrolysis. *J. Mater. Sci. Mater. Electron.* **1991**, *2*, 40–45. [CrossRef]
52. Doyan, A.; Susilawati; Imawanti, Y.D. Synthesis and Characterization of SnO_2 thin layer with a doping Aluminum is deposited on Quartz Substrates. *AIP Conf. Proc.* **2017**, *1801*, 020005.